Theor Chem Acc (2006) 116: 535–548
DOI 10.1007/s00214-006-0099-z

REGULAR ARTICLE

Esther Bordas · Coen de Graaf · Rosa Caballol
Carmen J. Calzado

Accurate determination of the electronic structure parameters of the spin ladder compounds $SrCu_2O_3$, $Sr_2Cu_3O_5$ and $CaCu_2O_3$

Received: 7 November 2004 / Accepted: 1 March 2005 / Published online: 14 February 2006

Abstract Ab initio embedded cluster calculations have been employed to calculate a large number of electronic structure parameters of three different spin ladders, namely $SrCu_2O_3$, $CaCu_2O_3$ and $Sr_2Cu_3O_5$. Using the iterative difference dedicated configuration interaction methodology, magnetic couplings J and hopping amplitudes t are determined for first to fourth nearest neighbors. In addition, the four-body cyclic exchange J_{ring} is extracted and the direct exchange K, the neutral-ionic hopping integral t_0 and the on-site repulsion U are calculated for first and second nearest neighbor copper ions. The substitution of these parameters in the pertubative superexchange relation $J = 2K - 4t_0^2/U$ yields magnetic coupling parameters in close agreement with the variational estimates. The spin ladders can be considered as an interpolation between the one-dimensional (1D) spin chains and the 2D antiferromagnets. Hence, results are compared with similar parameters in the spin chain Sr_2CuO_3 and the two-dimensional antiferromagnet La_2CuO_4.

PACS numbers 75.30.Et · 74.25.Jb · 75.10.Dg · 75.50.Ee

1 Introduction

The rapid increase of the dimensions of the exact Hamiltonian prohibits the ab initio study of collective properties in the copper oxide planes of the lamellar cuprates and other compounds as quasi one-dimensional (1D) spin 1/2 chains, or spin ladders. For this reason, the low-energy physics is often mapped onto a model Hamiltonian parameterized by a set of effective parameters. This largely reduces the computational cost and has been shown to be a very successful way to study the intriguing physics of the copper oxide compounds. One of the simplest model Hamiltonians contains two parameters, namely the nearest neighbor magnetic interaction parameter J and the hopping integral t, leading to the so-called t–J model [1]. This model is easily extended by considering not only the nearest neighbor interactions but also the interaction between centers that are more separated in space [2–4]. In this way, interactions along the diagonal of the plaquettes in CuO_2 planes, interplane or interchain interactions can be included in the model. The extension of the t–J model is, however, not limited to the next-nearest neighbor magnetic or hopping parameters, but parameters of different nature can also be included. One example is the four-spin cyclic exchange term. This interaction has been invoked to explain the large side band of the 0.4 eV peak observed in the lamellar cuprates [5,6]. The interaction has also been suggested to be of importance in the spin ladders [7–9]. The fitting of the magnetic susceptibility [10] and neutron scattering data [11] with just J_{rung} and J_{leg} leads to a ratio between the two magnetic interaction parameters of 0.5. This surprising result changes to a more isotropic ratio when the four-spin cyclic exchange is included in the analysis of the experimental data.

Despite the successes of the model Hamiltonian approach to explain and/or predict many details of the cuprate physics, it has the drawback that in some cases the effective model parameters are not easily derived from experiment. For compounds with just one dominant superexchange path, the magnetic interaction parameter can be accurately derived from neutron scattering or magnetic susceptibility data. However, for more complicated systems the result of the fitting of the experimental data can be dependent on the number and nature of interactions considered in the fitting as illustrated by the case of the spin ladders mentioned above. It is even more difficult to extract accurate estimates of the hopping parameters from experiment. The value of the nearest neighbor hopping parameter of 0.5 eV derived for $La_{2-x}Sr_xCuO_4$ is commonly extrapolated to other cuprates with similar Cu–O–Cu bonds. Although this is certainly not an absurd assumption, it is not completely clear to what extent this hopping parameter varies

E. Bordas · C. de Graaf(✉) · R. Caballol
Departament de Química Física i Inòrganica,
Universitat Rovira i Virgili, Marcel·lí Domingo, s/n.,
43007 Tarragona, Spain
E-mail: coen@urv.net

C.J. Calzado
Departamento de Química Física, Universidad de Sevilla, c/Prof. García González s/n, 41012 Sevilla, Spain
E-mail: calzado@us.es

from compound to compound. Similar considerations can be made about the next-nearest neighbor hopping interactions, which have been claimed to be involved in the formation of charge stripes in the CuO_2 planes of the lamellar cuprates [12–15].

An alternative way to obtain information about the magnitude of the effective model parameters is to perform electronic structure calculations. In many studies band structure density functional calculations are performed, where the electron–electron interaction is treated in the local density approximation (LDA). This means that the exchange-correlation part of the functional is taken from a model system corresponding to the non-interacting electron gas. In the case of the strongly correlated cuprates this approximation has rather important consequences. LDA predicts many cuprate compounds to be metallic, where experimentally a clear insulating character is observed [16–19]. It is by now well known that magnetic interaction parameters derived from LDA calculations do not reflect realistic values. For example, J(LDA) for La_2CuO_4 is more than 1 eV [20,21], while it is generally accepted (both confirmed from experimental and theoretical studies [22–27]) that this interaction is accurately parameterized by a J value of 0.13 eV. It is not very well established to what extent the hopping parameters derived from LDA calculations give an accurate parameterization of the dynamics of the holes.

Density functionals that introduce non-local terms do not improve upon the LDA results [21], while the application of hybrid functionals or LDA+U [28,29] introduces a parameter in the calculations (the amount of exact Fock exchange and the on-site repulsion, respectively) that can be optimized to give the desired result [30–32]. An alternative theoretical scheme is offered by the wave function based methods, which allow for a rigorous treatment of the electron correlation effects. It is generally not possible to go beyond the Hartree–Fock level in a band structure calculation with a wave function based computational scheme, but the embedded cluster model approach avoids this limitation and will be applied here to derive ab initio electronic structure parameters for the two-leg spin ladder compounds $CaCu_2O_3$ and $SrCu_2O_3$ and the three-leg ladder compound $Sr_2Cu_3O_5$.

The spin ladder compounds interpolate between the 1D spin chains and the 2D antiferromagnetic planes found in the parent compounds of the superconductors and, hence, form a very interesting object of study [33–35]. Experimental data and theoretical studies with model Hamiltonians indicate that the transition from 1D to 2D is far from smooth. Even-legged ladders exhibit a spin gap and finite spin–spin correlations, whereas the odd-legged ladders behave as effective 1D spin chains, i.e. no spin gap and no spin ordering when $T \rightarrow 0$ [36–38]. There are, however, several points that need to be clarified or studied in more depth. In the first place, as has already been mentioned before, it is not completely clear how J_{rung} relates to J_{leg}. Secondly, it is almost always assumed that the spin ladders can be treated as isolated systems, although the interladder interactions have been claimed to be significant by some authors [39]. Furthermore, it is interesting to have independent estimates of the different hopping parameters and the four-spin cyclic exchange in the three compounds in order to assess the dependence of these parameters on the geometry of the Cu–O–Cu bonds. In $SrCu_2O_3$ and $Sr_2Cu_3O_5$ these bonds have angles of approximately 180° (rung and leg) or close to 90° (interladder), whereas in $CaCu_2O_3$ the deformation of the Cu_2O_3 planes causes Cu–O–Cu angles of 123°.

2 Definition of the model parameters

In the present work, we extend previous ab initio studies on the copper oxide spin ladders [39,40] by parameterizing an extended model Hamiltonian that includes up to fourth neighbor magnetic interactions and hopping parameters. Moreover, we calculate the cyclic exchange J_{ring}, the direct exchange K, the neutral-ionic hopping integral t_0 and the on-site repulsion U. Figure 1 illustrates the interactions that we consider in this study. Some of the results have also been discussed in previous papers. The work by de Graaf et al. focuses on the ratio between the magnetic interactions along the leg and rung in $SrCu_2O_3$[39], and the study of Calzado et al. [40] addresses the size of the four-spin cyclic exchange in the spin ladders. The scope of the present paper is to give a complete detailed description of the electronic structure parameters that control the low-energy physics of $SrCu_2O_3$, $CaCu_2O_3$ and $Sr_2Cu_3O_5$.

The first neighbor interaction parameters J_{inter} and t_{inter} measure the strength of the interladder coupling. The rectangular Cu–O–Cu bonds suggest that this interaction is rather weak and ferromagnetic in nature. In the case of the strontium compounds, the second neighbor interactions J_{rung}, J_{leg}, and the respective ts take place along linear Cu–O–Cu bonds and are the strongest present in these spin ladder compounds. Their relative size is controversial and will be discussed in this paper. For the calcium ladder, a strong spatial anisotropy is expected in its second neighbor interactions. The bending of the Cu–O–Cu bond along the rung makes the interaction along the leg much larger than along the rung. The interactions between third neighbors (J_{diag} and t_{diag}) and fourth neighbors (J'_{leg}, J'_{rung} and the respective ts) are small, but probably important corrections. In the three-leg ladder compound $Sr_2Cu_3O_5$ we distinguish between inner and outer legs as indicated in Fig. 1.

Finally, K, t_0 and U have been calculated for first (interladder) and second (rung + leg) neighboring copper ions.

Interactions between different ladder planes are expected to be very small for the planar spin ladder compounds. The relative orientation of the CuO_4 units is similar to that in the spin chain compounds Ca_2CuO_3 and Sr_2CuO_3. For these compounds the nearest neighbor interchain magnetic coupling has been estimated to be as small as 1 meV [41]. Therefore we do not consider such interactions in the present study. The situation is somewhat different in the buckled Ca ladder compound, for which significant interplane interactions have been suggested based on periodic LDA calculations [42]. In

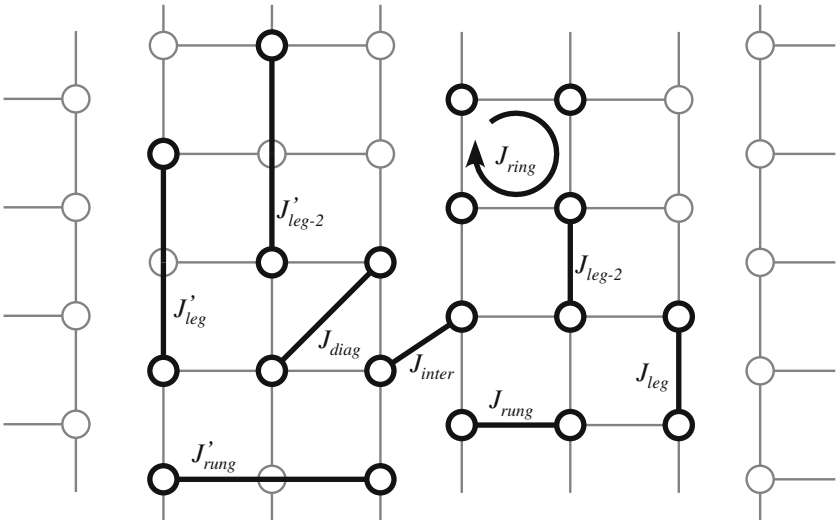

Fig. 1 Schematic view of the Cu_2O_3 layer in $Sr_2Cu_3O_5$. *Open circles* represent Cu ions, oxygen ions (not shown) are located halfway on the *thin gray lines* that connect coppers. The different interactions between the Cu ions are indicated with *black lines*. The same nomenclature is used for the hopping parameters

the discussion of the results we will shortly review some results of ab initio calculations on this subject [91].

3 Computational approach

3.1 Material model

The local nature of the interactions under study allows us to model the material within the so-called cluster model approach. There exist by now a large amount of evidence of the reliability of the cluster model approach to calculate such interactions. Several studies have been published that contrast the cluster results with periodic calculations. In all cases, the calculated values are very similar given that the approximation to the *N*-electron wave function is identical in both approaches [43–46].

A small cluster is cut from the crystal and is treated with state-of-the-art quantum chemical techniques to obtain highly correlated *N*-electron wave functions. This cluster contains the copper ions involved in the interaction and its direct oxygen neighbors. To include the remainder of the crystal in the material model, the cluster is embedded in a static potential that accounts for the long-range electrostatic interactions with a point charge approximation and the short-range interaction between cluster and immediate surroundings by means of properly designed total ions potentials (TIPs) [47].

Figure 2 shows the cluster model to extract the first neighbor interactions in $SrCu_2O_3$. The quantum chemically treated region corresponds to a Cu_2O_6 cluster, which is embedded in six TIPs for Cu^{2+}, eight TIPs for Sr^{2+} and point charges (only a small fraction is shown in Fig. 2). The clusters used to extract the other interactions have been constructed in a similar fashion and are tabulated in Table 1. Although a cluster with just two copper ions seems the natural choice to calculate the magnetic interaction along the leg, the inclusion of the copper ion on the neighboring leg has a relatively large effect on the magnetic coupling of the copper ions along the leg and, therefore, we use the triangular Cu_3O_8 cluster to calculate this interaction. In the discussion of the results we will come back to this point.

Structural parameters have been taken from the literature [48,49] (D.C. Johston, M. Troyer, S. Miyahara, D. Lidsky, K. Veda, M. Azuma, Z. Hirola, M. Takano, M. Isobe, Y. Veda et al., unpublished). For $SrCu_2O_3$, we compare the results obtained from the original structural determination by Hiroi et al. [48] and the refinement proposed by Johnston et al. (unpublished).

3.2 Approximation to the exact *N*-electron wave function

The strong electron correlation effects are incorporated in the electronic wave function by state-of-the-art quantum chemical methods. Here, we opt for the difference dedicated configuration interaction (DDCI) scheme, specially designed to calculate energy differences with high accuracy [50,51]. Over the last decade, this method has been successfully applied to calculate magnetic interaction parameters in biradicals, inorganic molecules and a wide family of ionic insulators including the parent compounds of the high-T_c superconductors (see Refs. [24, 46, 52–56] and references therein).

The reference wave function for the DDCI is obtained by distributing the unpaired electrons in all possible ways over the Cu-$3d_{x^2-y^2}$ orbitals, i.e. a complete active space CI (CASCI), which corresponds to the well-known Anderson model with unscreened parameters. The open-shell orbitals are the active or magnetic orbitals, while all other orbitals will be referred to as inactive or virtual orbitals, depending on the occupation in the reference wave function. The fact that U is

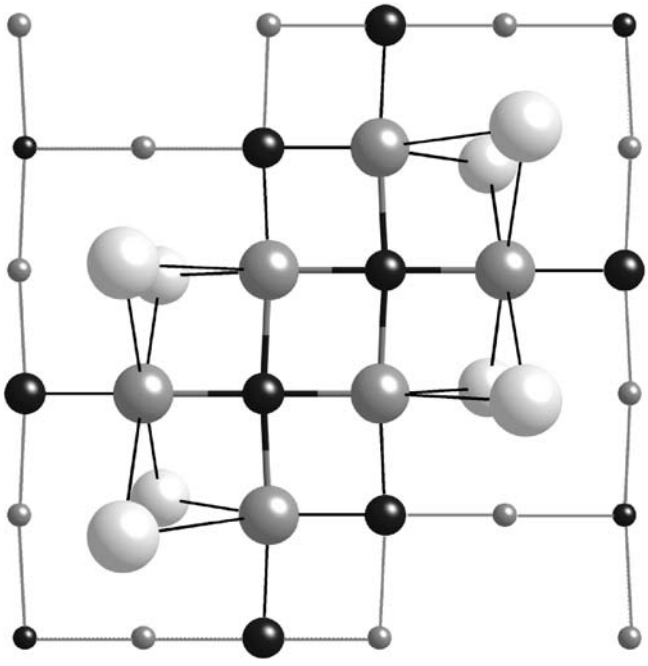

Fig. 2 Cu_2O_6 cluster embedded in TIPs and point charges (only partially shown) used to calculate J_{inter} and t_{inter} in $SrCu_2O_3$ with the refined structure. *Black spheres* represent Cu ions, *gray spheres* represent O and *light gray spheres* represent Sr. *Large spheres* connected by *black-gray lines* are cluster atoms, TIPs are connected to the cluster atoms by *thin black lines* and *small spheres* are point charges

Table 1 Cluster models used to extract the different magnetic interactions between copper ions and the same applies for the hopping parameters

Number of Cu centers	Cluster model	Interaction
Two centers	Cu_2O_6	J_{inter}
	Cu_2O_7	J_{rung}, $J_{leg\text{-}2}$
Three centers	Cu_3O_8 (triangular)	J_{leg}
	Cu_3O_{10} (linear)	J'_{leg}, J'_{rung}, $J'_{leg\text{-}2}$
Four centers	Cu_4O_{12} (rectangular)	J_{diag}, J_{ring}

overestimated by a factor of 3 in the CASCI wave function explains that the magnetic interaction parameters obtained at this level are far too small and improvement is required. The DDCI space is constructed by all single and double replacements of electrons with respect to the reference under the restriction that at least one active orbital is involved. This precisely excludes the double replacements from the inactive to the virtual orbitals, which are most numerous and hence largely reduces the computational demand of the calculation. The justification of this restriction lies in the observation that up to second-order perturbation theory the double replacements from inactive to virtual orbitals shift all diagonal elements in the CI matrix by the same amount and do not contribute to the off-diagonal elements. Hence, these double replacements do not contribute to the energy difference of the electronic states.

The choice of the orbitals to construct the Slater determinants that form the basis of the CI space is somewhat arbitrary. A common choice is to take the Hartree–Fock orbitals of the spin state with highest multiplicity. This can, however, bias the results and to eliminate any dependence of the results on the orbital choice, we adopt an iterative scheme of the DDCI method (IDDCI) [57]. After the diagonalization of the CI space, the one-particle density matrices of the electronic states involved in the interaction are averaged and diagonalized. The DDCI procedure is repeated with the resulting average natural orbitals until convergence in the energy differences of the electronic states is obtained.

For the four-center cluster used to calculate J_{ring}, the DDCI expansion is too large to be handled by present computer resources. Therefore, a more approximate computational scheme has been applied. The reference wave function is extended with oxygen to copper charge transfer configurations, but the CI space is built from single excitations only. This extended-CAS + singles method gives approximately the same results for the two-center cluster as the more rigorous DDCI but the computational cost is much lower [58–60].

Finally, to expand the one-electron functions (or the so-called orbitals), we use an atomic natural orbital basis set with (5s, 4p, 3d) contracted Gaussian type functions for Cu and (4s, 3p) contracted functions for O [61,62]. Calculations have been performed with the MOLCAS 5.4 Quantum Chemistry software package [63] and the CASDI code [64].

3.3 Extraction of the effective parameters

With the *N*-electron wave functions of Sect. 3.2 as approximations to the eigenfunctions of the exact non-relativistic Hamiltonian of the cluster models defined in Sect. 3.1, it is possible to calculate all the electronic structure parameters

discussed above. In the two-center and three-center clusters, the magnetic interaction parameters are directly related to the energy differences of the electronic states that arise from the different couplings of the spin moments localized on the Cu ions. The mapping of the energy eigenvalues onto the eigenvalues of the Heisenberg Hamiltonian defines J_{rung}, $J_{\mathrm{leg}-2}$ and J_{inter} as the energy difference of the singlet and the triplet: $E(\mathrm{S}) - E(\mathrm{T})$. The Heisenberg Hamiltonian for the linear and triangular three-center clusters is

$$\hat{H} = -J_1(\hat{S}_1\hat{S}_2 + \hat{S}_2\hat{S}_3) - J_2\hat{S}_1\hat{S}_3. \quad (1)$$

The energy eigenvalues of the electronic eigenstates are related to J_1 and J_2 by the following relations: $J_1 = 2/3(E_{\mathrm{D1}} - E_{\mathrm{Q}})$ and $J_2 = J_1 - (E_{\mathrm{D1}} - E_{\mathrm{D2}})$, with E_{D1}, E_{D2}, and E_{Q} the energy eigenvalues of the two doublet and quartet states, respectively. For the linear clusters, J_1 and J_2 correspond to J_{leg} and J'_{leg}, respectively. In the case of the triangular cluster, J_1 and J_2 correspond to J_{inter} and J_{leg}. The calculation of the hopping parameters discussed in Sect. 4.2 requires the use of doped clusters, i.e. with one electron less compared to the calculation of the magnetic interaction parameters. When the cluster with two magnetic centers exhibits an inversion center, ts are obtained from half the energy difference of the electronic states in which either the bonding or anti-bonding combination of the magnetic orbitals is occupied [23].

To extract the other electronic structure parameters, the energy eigenvalues are not sufficient and information about the wave function is also necessary. For this purpose the effective Hamiltonian theory is applied, in which the IDDCI wave functions are projected onto a simple valence effective Hamiltonian. The matrix elements of this effective Hamiltonian can be related to the electronic structure parameters as described in Refs. [54, 58, 59].

4 Results

4.1 Magnetic interaction parameters

4.1.1 Leg interactions

Starting with the second neighbor interactions, we observe rather similar magnetic coupling along the legs of the ladders in all three compounds, see Table 2. Given the similarity of the Cu–O–Cu exchange path, this is not a surprising observation. Furthermore, we do not see a significant difference in J_{leg} comparing the idealized structure of $SrCu_2O_3$ to the refinement reported by Johnston et al. (unpublished). As stated in Sect. 3.1, we find a moderate cluster size dependency of the interaction along the leg. Adding a third copper ion on the same leg hardly affects J_{leg} as observed in many other applications. However, adding the nearest Cu^{2+} on the leg of the next ladder has a significant effect on J_{leg}, which decreases by approximately 17%. To check the convergence of J_{leg} with the cluster size, we constructed a four-center cluster with two copper ions on one leg and two on the leg of the neighboring ladder (see Fig. 3).

Table 2 Magnetic coupling parameters (in meV) for $SrCu_2O_3$, $CaCu_2O_3$ and $Sr_2Cu_3O_5$

	$SrCu_2O_3$		$CaCu_2O_3$	$Sr_2Cu_3O_5$
	Idealized	Refined		
J_{leg}	−155	−155	−139	−190/− 186
J_{rung}	−150	−125	−11.5	−175
J_{inter}	34.9	35.5	28.2	34.5
J'_{leg}	−2.7	−2.7	<0.1	−4.0/− 3.6
J'_{rung}				−3
J_{diag}	−13		−0.4	−14

The two values for J_{leg} and J'_{leg} in case of $Sr_2Cu_3O_5$ correspond to the outer leg and inner leg (leg-2 in Fig. 1), respectively. All results correspond to IDDCI values, except J_{diag}, which is given at the extended-CAS + singles level.

Table 3 J_{leg} (in meV) for $SrCu_2O_3$ with the refined structure obtained with two-center, three-center and four-center clusters

	CASSCF	CASPT2	DDCI1	DDCI2	DDCI	IDDCI
Two centers	−34.3	−130.6	−91.1	−96.5	−158.8	−186.0
Three centers	−32.8	−123.8	−86.7	−92.4	−122.2	−154.9
Four centers	−32.5	−122.3	−87.9	−93.0		

In Table 3, we compare the results of several approximations for the N-electron wave function, because the DDCI calculation is not feasible for the cluster with four Cu centers. The complete active space second-order perturbation theory (CASPT2) method provides a perturbational treatment of the electron correlation effects and has been proven to give a rather good description of the magnetic coupling in transition metal (TM) materials [52]. DDCI1 and DDCI2 diagonalize subsets of the complete DDCI space and commonly reproduce between 50 and 70% of the full DDCI value. At all levels of approximation, the magnetic coupling parameter reduces going from the two-center cluster to the triangular three-center cluster but stays nearly constant when a fourth Cu center is added to the cluster. Extrapolating these findings to the DDCI calculations, we conclude that the DDCI value of the three-center cluster is free of cluster size effects. Similar effects occur for J_{leg} in $CaCu_2O_3$ and $Sr_2Cu_3O_5$. Cluster size effects have been studied before in other cuprates (Li_2CuO_2, Sr_2CuO_3 and La_2CuO_4) and nickel compounds (NiO, $KNiF_3$ and K_2NiF_4), but in none of these cases a significant effect has been found [41,59,65,66]. Also in the present study, we not only performed a cluster size study for J_{leg} but also for J_{rung} in $Sr_2Cu_3O_5$. In this case, the results are almost identical for the two-center cluster (half of the rung) and the three-center cluster containing a complete rung. Hence, the overestimation of J_{leg} in the two-center cluster for the spin ladders seems to be a special case, probably due to the appearance of a third Cu atom very close to the Cu–O–Cu exchange path along the leg.

In an attempt to clarify the cluster size effect due to the third copper (center c in Fig. 3), we analyze two possible mechanisms that could affect J_{leg}. In the first place, we verify the validity of the embedding of the two-center cluster by replacing the third copper center with a diamagnetic Zn^{2+} cation. The ionic radius of Zn^{2+} is very similar to the one of

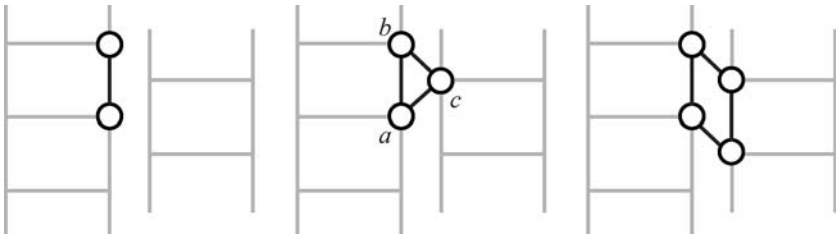

Fig. 3 Schematic representation of the two, three and four-center clusters used to investigate the cluster size convergence of J_{leg}

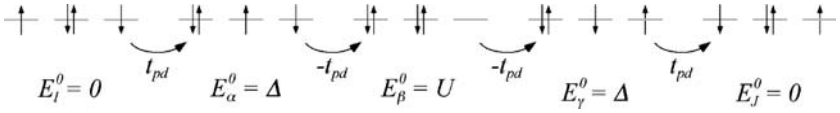

Fig. 4 Kinetic exchange mechanism between two copper ions on the same leg. Interaction matrix elements between the subsequent states are indicated *below the arrows*. Relative energies are also shown

Cu^{2+} and, hence, this diamagnetic cation gives a good representation of the charge distribution of a real Cu^{2+} ion without having to deal with unpaired electrons. It can be argued that the representation of center c with a TIP in the two-center clusters is too approximate being located so close to the magnetic exchange path. Nevertheless, we do not observe any significant difference in J_{leg} with the Cu-TIP replaced by a real Zn^{2+} ion.

Having established that the reduction of J_{leg} cannot be ascribed to the embedding, we determine how this additional copper center can modify the exchange path between the two copper centers on the same leg (centers a and b in Fig. 3). As discussed in Ref. [67], the charge transfer from the ligand orbital to the metal gives important contributions to the kinetic exchange at fourth-order perturbation theory in bicentric systems. Therefore, we will analyze here the additional contributions of this type that come from the third metal center. We start by shortly reviewing the well-known kinetic exchange process of the two-band Anderson model, where only the centers a and b and the bridging ligand are involved. The major contribution to the kinetic exchange between these centers arises from the process schematically depicted in Fig. 4.

Since all intermediate determinants are external to the model space S, we only have to consider the following term of the complete fourth-order perturbation theory expression to estimate the sign and magnitude of the pathways:

$$\sum_{\alpha\notin S}\sum_{\beta\notin S}\sum_{\gamma\notin S}\frac{\langle\Phi_I|\hat{V}|\Phi_\alpha\rangle\langle\Phi_\alpha|\hat{V}|\Phi_\beta\rangle\langle\Phi_\beta|\hat{V}|\Phi_\gamma\rangle\langle\Phi_\gamma|\hat{V}|\Phi_J\rangle}{(E_J^0-E_\alpha^0)(E_J^0-E_\beta^0)(E_J^0-E_\gamma^0)}, \tag{2}$$

where Φ_I corresponds to the $|ll\underline{a}\underline{b}|$ determinant and Φ_J to the $|ll\underline{b}\underline{a}|$ determinant. The interaction matrix elements along the pathways are obtained using the definitions in Fig. 5 of the effective hopping parameters: $\langle a|\hat{H}|l\rangle = -\langle b|\hat{H}|l\rangle = t_{\mathrm{pd}}$. With this parameterization, the nominator is equal to t_{pd}^4. Expressing the relative energies of the intermediate determinants with respect to the final determinant Φ_J in terms of the on-site repulsion U and the ligand to metal charge transfer energy Δ, the denominator in Eq. 2 for the pathway

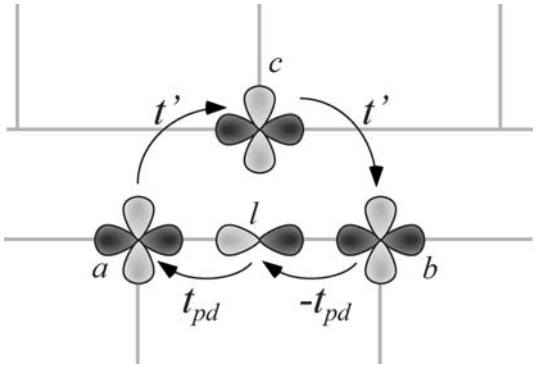

Fig. 5 Definition of the hopping parameters used in the fourth-order perturbation analysis of the changes in the kinetic exchange due to the third copper ion

in Fig. 4 is given by $(-\Delta)(-U)(-\Delta) = -\Delta^2 U$. The final perturbative expression for the kinetic exchange contribution to the magnetic coupling is therefore $-4t_{\mathrm{pd}}^4/\Delta^2 U$ (the factor four is due to the fact that there are four possible pathways that connect $|ll\underline{a}\underline{b}\rangle$ and $|ll\underline{b}\underline{a}\rangle$), in accordance with the usual understanding that this effect gives an antiferromagnetic contribution to the magnetic coupling between the two copper centers (see also Sect. 4.3).

The analysis for the three-center cluster is somewhat more involved, but follows exactly the same reasoning. Starting from the $|ll\underline{a}\underline{b}\underline{c}|$ determinant, there are 12 four-step pathways to reach the $|ll\underline{b}\underline{a}\underline{c}|$ determinant involving center c. Figure 6 schematizes the six pathways in which the electron movement is clockwise and Fig. 7 denotes the other six pathways with anti-clockwise electron movement.

The hopping from an electron involving center c is parameterized as $\langle a|\hat{H}|c\rangle = \langle b|\hat{H}|c\rangle = t'$ (see Fig. 5). In the determination of the sign of the nominator one should carefully take into account the permutations in the respective determinants. In the figures of the clockwise and anti-clockwise pathways, we denote the interaction matrix elements following the procedure of maximal coincidence of the two determinants involved. For example the upper

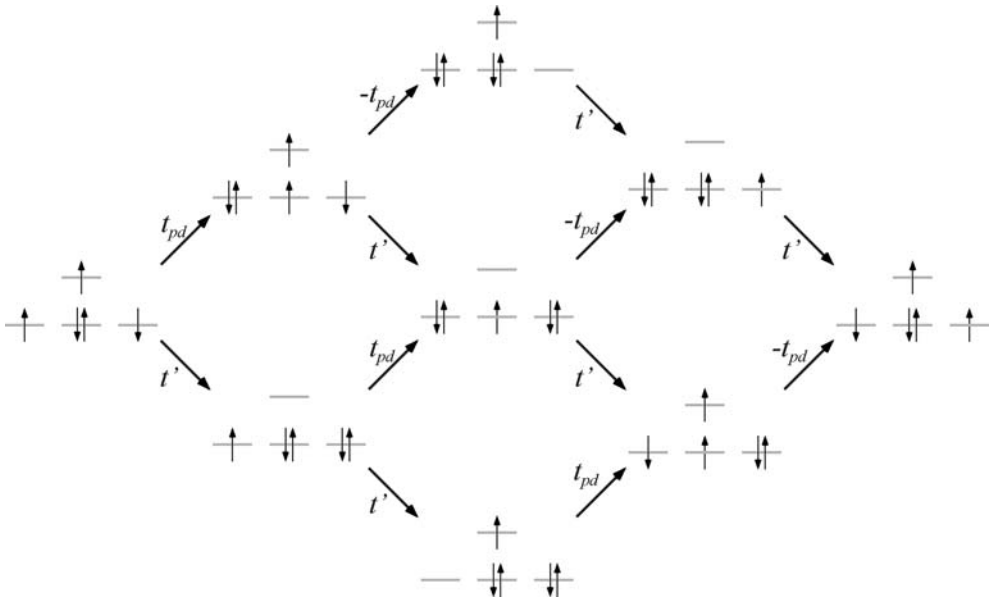

Fig. 6 Four-step pathways with clockwise electron movement

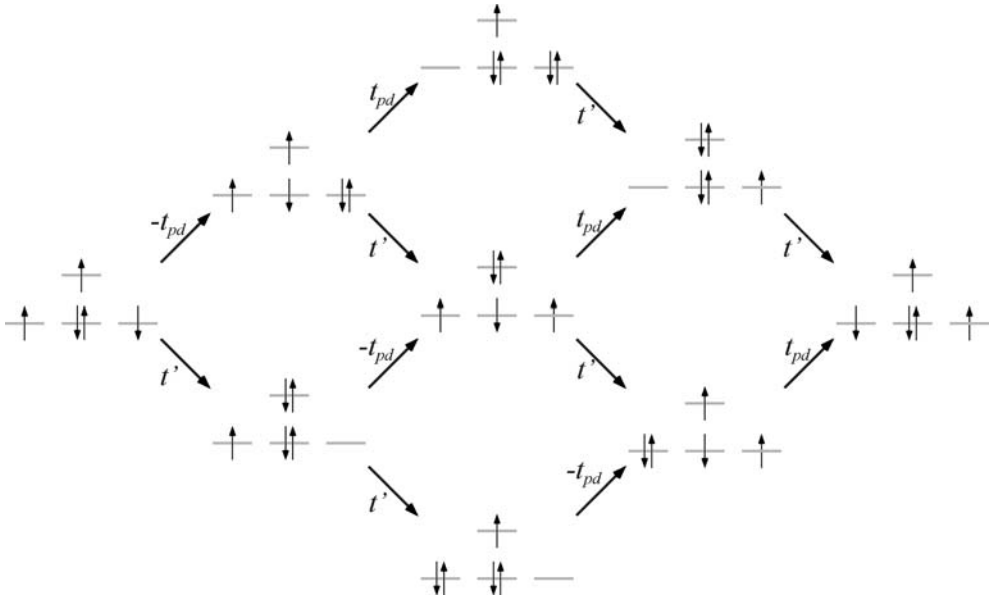

Fig. 7 Four-step pathways with anti-clockwise electron movement

anti-clockwise pathway considers the following matrix elements: $\langle l\underline{l}a\underline{b}c|\hat{V}|b\underline{l}a\underline{b}c\rangle = -t_{\mathrm{pd}}$; $\langle b\underline{l}a\underline{b}c|\hat{V}|b\underline{l}l\underline{b}c\rangle = t_{\mathrm{pd}}$; $\langle b\underline{l}l\underline{b}c|\hat{V}|b\underline{l}l\underline{c}c\rangle = t'$; $\langle b\underline{l}l\underline{c}c|\hat{V}|b\underline{l}l\underline{a}c\rangle = t'$. This leads to $-t_{\mathrm{pd}}^2 t'^2$ for all six anti-clockwise pathways. However, to convert the final determinant in the desired form $|ll\underline{b}\underline{a}c|$ one needs to permute b and l, causing a change in the sign of the overall expression, and hence a positive nominator. The same holds for the other five anti-clockwise pathways.

For the six clockwise pathways, the nominator is $-t_{\mathrm{pd}}^2 t'^2$. An even number of permutations is required to get the desired Φ_J, and therefore these nominators do not change sign and remain negative. Remembering that the denominator in Eq. 2 is always negative, the clockwise pathways decrease the kinetic exchange leading to a more ferromagnetic J_{leg}, while the anti-clockwise pathways enhance the kinetic exchange and lead to a more effective magnetic coupling along the leg.

Since the absolute value of the nominators is the same in all cases, the relative importance of the different pathways can only be assessed through the denominators. As before, we express the relative energies in terms of U and Δ, which implies the assumption that Δ is equal for charge transfer from the ligand to any of the three metal centers. Furthermore, we neglect the contribution to the energy of the

magnetic coupling between unpaired electrons in this perturbative analysis. It can readily be seen that the only difference between the two diagrams arises from the determinant in the middle. The energy of the $|a\underline{a}b\underline{b}l|$ determinant intervening in four of the six clockwise pathways lies at $U + \Delta$, while the $|c\underline{c}a\underline{l}b|$ determinant, which appears four times in the anti-clockwise pathways, has a relative energy of only Δ. From this, we expect a larger contribution to the kinetic exchange of the anti-clockwise pathways, which would lead to a stronger antiferromagnetic coupling along the leg. This is opposite to what we observe comparing the two-center with the three-center cluster (see Table 3). Hence, we conclude that the reduction of J_{leg} is caused by other electron correlation processes discussed in Ref. [67], which become very cumbersome to analyze with perturbation theory arguments.

4.1.2 Rung interactions

The results in Table 2 show that the interactions across the rung are very different in the spin ladders with Sr and the one with Ca. The bending of the Cu–O–Cu angle causes a drastic decrease of the magnetic coupling along the rung in $CaCu_2O_3$. Actually the decrease is such that this compound is better understood as containing quasi-1D spin 1/2 chains with weak interchain interactions, J_{rung} and J_{inter}. Another remarkable feature is the noticeable difference between the magnetic coupling in the idealized structure of $SrCu_2O_3$ and the refined one. In the latter structure, we calculate a value which is almost 15% smaller than in the idealized structure. At first sight this is rather surprising since geometrical parameters as the Cu–O–Cu bond angle and the Cu–O bond length hardly change the exchange path along the rung, whereas there are small changes on the leg, for which the magnetic coupling is constant. The explanation can be found in the Madelung potential at the atomic centers listed in Table 4. The potential is calculated assuming formal charges for all atoms, i.e. 2+ for Cu and Sr and 2− for O. In a simple ionic model, the difference in Madelung potential between the copper and oxygen sites Δ_{Mad} is a measure of the charge transfer energy. For smaller absolute difference, a lower oxygen to metal charge transfer energy is expected and hence a larger magnetic coupling. Table 4 shows that this energy difference increases both for the leg and rung oxygen, but the change is much more pronounced for the rung oxygen, explaining the relatively large decrease of J_{rung} for the refined structure.

Table 4 $SrCu_2O_3$ Madelung potential (in eV) at atomic sites for idealized and refined structures

Atom	Idealized	Refined
Cu	−24.38	−24.97
Sr	−19.67	−18.98
O_r	21.35	22.09
O_l	22.45	22.25
$\Delta_{\text{Mad}}(O_r–Cu)$	45.73	47.06
$\Delta_{\text{Mad}}(O_l–Cu)$	46.82	47.21

O_r and O_l refer to the oxygens located on the rung and leg, respectively

4.1.3 Other magnetic interactions

Although the Cu–Cu distance is smallest for the interladder interaction, its magnitude is much smaller than the interaction along the leg or rung of the spin ladders. The Cu–O–Cu bond angle of approximately 90° makes that two orthogonal O-2p orbitals are involved in the superexchange process, instead of only one for bonding angles around 180°. This causes a much less effective superexchange and hence a smaller magnetic coupling. Moreover the short Cu–Cu distance increases the direct exchange between the copper ions, which explains the ferromagnetic character of the interladder interaction in all three spin ladders. The ratio between the interladder coupling and the coupling along the legs never exceeds the value of 0.2. It has been shown that below this limit, the interladder interaction does not significantly affect the values of the intraladder interactions when fitting to experimental data (Johnston et al., unpublished).

The only remaining magnetic interaction of significant magnitude is the diagonal coupling between Cu on different legs of the same ladder. Several studies have been concerned with the influence of this coupling on the phase diagram of the spin 1/2 ladders [68–70]. LDA+U calculations indicate that this coupling in the spin ladders is ferromagnetic (Johnston et al., unpublished) in contrast to what is found, both experimentally and theoretically, in the closely related 2-D antiferromagnet La_2CuO_4, for which this interaction is antiferromagnetic with an amplitude of about −5 to −10 meV [58,59,71]. Our ab initio values for J_{diag} indicate that this is also the case for the planar spin ladders, whereas it is very weak for $CaCu_2O_3$. We conclude that in the study of the phase diagram of spin 1/2 ladders, a realistic set of parameters should include a moderate antiferromagnetic diagonal coupling. The other couplings are of the order of a few millielectron volts and can probably be neglected.

4.2 Hopping parameters from doped clusters

The second group of calculations addresses the size of the parameters that control the mobility of holes doped into the lattice. The 2D parent compounds of the high T_c superconductors are commonly doped with holes by replacing some of the trivalent ions (e.g. La^{3+} or Y^{3+}) by divalent ions as Sr^{2+}. Alternatively, interstitial oxygen ions can be introduced to create holes in the copper oxide planes. Actually, the spin ladder systems studied here are not commonly submitted to this type of doping. The most common experimental realizations of hole-doped ladder systems are found in the incommensurate $Sr_{14-x}Ca_xCu_{24}O_{41}$ compounds, for which superconductivity has been found for x=13.6 [72].

It is well known that the holes are not localized on the copper sites but have a more delocalized character and extend onto the nearest neighbor oxygens. This behavior is correctly reproduced in ab initio cluster calculation as demonstrated by Calzado et al. [25] for holes in La_2CuO_4. In line with these results, we find a similar delocalization of the holes onto the oxygens for the spin ladders. Beside this qualitative

validation of the cluster model to correctly describe doping in ionic copper oxide structures, it is also convenient to have a more quantitative test of the cluster model validity. In previous applications of this approach it was already shown that quantum chemical cluster calculations satisfactorily reproduce the generally accepted value of $t = -500$ meV for La_2CuO_4 and related lamellar cuprates [23,25,46]. Additional evidence has been given in a study of the spin chains Ca_2CuO_3 and Sr_2CuO_3, where it was found that the LDA values of cluster and periodic calculations are very similar [41]. Moreover, it has been shown that t is relatively insensitive to the computational strategy applied; LDA, CASSCF, DDCI (and other schemes) give approximately the same result [41, 73]. This allows us to assess the validity of the cluster model by comparing our IDDCI estimate for t_{rung} in $CaCu_2O_3$ with the recently published estimate of the same parameter based on periodic LDA calculations [42].

Table 5 lists the IDDCI hopping parameters for the three ladder systems. The largest hopping parameters are found along the (almost) linear Cu–O–Cu bonds, i.e. along the legs in all three ladder systems and along the rungs in the Sr ladders. The values are comparable to the hopping along similar Cu–O–Cu bonds found in the 2D antiferromagnets La_2CuO_4 [25] and related cuprates [46]. The buckling of the Cu_2O_3 planes in the Ca compound reduces the hopping amplitude of the holes along the rung with a factor of about 2.5. The loss of the linearity in the Cu–O–Cu linkage reduces the overlap between the metal-centered orbitals that accommodate the unpaired electron. The interladder hopping amplitudes are still smaller in line with the decreasing Cu–O–Cu angle.

Our IDDCI estimate of -240 meV for t_{rung} in $CaCu_2O_3$ is in remarkably good agreement with the periodic LDA value of $\sim$ 250 meV recently reported by Kim et al. [42]. These authors also find important hopping parameters along the c-axis, i.e. between ladders in different planes. The fit of the LDA band structure results in a t_c of $\sim$ 125 meV. DDCI cluster calculations reported in [91] give $t_c = 134$ meV and confirm the importance of the hopping between different ladder planes. Nevertheless, the conclusion of Kim et al. that this relatively large hopping leads to important magnetic coupling along the c-axis was not confirmed in the DDCI study. The J-values for magnetic coupling along the c-axis are less than 1 meV.

Table 5 IDDCI effective hopping parameters (in meV) for $SrCu_2O_3$, $CaCu_2O_3$ and $Sr_2Cu_3O_5$

	$SrCu_2O_3$		$CaCu_2O_3$	$Sr_2Cu_3O_5$
	Idealized	Refined		
t_{leg}	−653	−655	−599	−638/− 650
t_{rung}	−609	−561	−240	−658
t_{inter}	103.3	165	141	103
t'_{leg}		−51	−18	−18/− 76
t'_{rung}				−50

The two values for t_{leg} and t'_{leg} in case of $Sr_2Cu_3O_5$ correspond to the outer leg and inner leg (leg-2 in Fig. 1), respectively

4.3 Other electronic structure parameters

The valence Hamiltonian descriptions of magnetic coupling by Anderson [74], Hay et al. [75] and Kahn and Briat [76] are based on the balance between the ferromagnetic contribution J_F of the direct exchange between the magnetic moments and the antiferromagnetic contribution J_{AF} due to kinetic exchange of the unpaired electrons:

$$J = J_F + J_{AF} = 2K - \frac{4t_0^2}{U}. \quad (3)$$

As shown in previous studies [53,54], the two effects can be accurately parameterized by projecting the IDDCI wave functions onto an effective Hamiltonian. The model space of this effective Hamiltonian consist of four electronic states, namely the low-energy singlet and triplet states with dominant contributions from the neutral determinants and two excited singlet states characterized as ionic states (see Ref. [54] for a more comprehensive description of the model space). The neutral states are easily identified among the lowest IDDCI roots, but the situation is quite more complicated for the excited singlet states. These ionic singlet states are expected to lie approximately 6 eV above the neutral states (the energy difference is related to U, which is typically 6 eV for copper oxides). Many other states may appear in this energy region and the norm of the projection may become rather small. Eventually, several states with almost equal energy eigenvalues may have rather similar norms in the model space. Hence, one can conclude that although the relative energy of the excited singlets is a reliable quantity, the coefficients of the projection on the model space can be affected by the mixing with other states.

The application of Bloch's effective Hamiltonian formulation [77] requires the knowledge of the relative energies and the coefficients of the neutral and ionic determinants of all four states in the model space. Hence, the Bloch Hamiltonian transfers the maximum amount of information from the total space into the model space, although the resulting Hamiltonian is non-hermitic, which complicates the interpretation of the matrix elements. Due to difficulties with the identification of the excited singlet states, the Bloch Hamiltonian for the present systems is strongly non-hermitic and the resulting parameters might be affected by the poor definition of the coefficients of the excited singlet states. Therefore, we only list the results obtained with the Gram-Schmidt effective Hamiltonian. This formulation avoids the non-hermiticity of the Bloch Hamiltonian and only uses the relative energy of the excited singlets, since the coefficients are imposed by orthogonality requirements. Furthermore, it does not force to fix one of the parameters from the start as is the case for the intermediate effective Hamiltonian [78].

Defining a and b as orthogonal magnetic orbitals localized on the magnetic centers A and B, respectively, t_0 is the matrix element between the neutral and ionic valence bond determinants:

$$t_0 = \frac{1}{4}\langle (a\underline{b} + b\underline{a})|\hat{H}|(a\underline{a} + b\underline{b})\rangle, \quad (4)$$

and U is defined as the difference of the energy expectation values of the ionic and neutral valence bond determinants:

$$U = \frac{1}{4}[\langle(a\underline{a} + b\underline{b})|\hat{H}|(a\underline{a} + b\underline{b})\rangle - \langle(a\underline{b} + b\underline{a})|\hat{H}|(a\underline{b} + b\underline{a})\rangle]. \quad (5)$$

The hopping integral t_0 should not be confused with the hopping amplitudes derived in Sect. 4.2 for the doped clusters. Results in Table 6 show that the t_0 values for the neutral clusters are indeed different from the hopping parameters listed in Table 5. In general smaller values are obtained for the neutral clusters and especially significant is the reduction by a factor of approximately two of the hopping parameter for the interladder interactions.

The largest Ks are obtained for the interladder interactions. In this case the two copper ions are least separated (<3.0 Å) and hence have the largest direct exchange. The interatomic Cu distance along the leg and rung is much larger (≈ 4.0 Å), which is reflected in a significantly smaller K. In between these two extremes, there is $K = 8.8$ meV for the rung in $CaCu_2O_3$. The two copper ions on the same rung are separated by only 3.3 Å because of the buckling of the ladder planes.

The three-legged compound $Sr_2Cu_3O_5$ gives rise to slightly different electronic structure parameters along inner and outer legs. Because the copper ions on the rung are not identical, the ionic determinants $|a\underline{a}\rangle$ and $|b\underline{b}\rangle$ are no longer degenerate in this case. Therefore, Table 6 also lists two values for t_0 and U for the rung in $Sr_2Cu_3O_5$.

With the ab initio values of the parameters in Eq. 3 at hand, it can be tested to what extent this perturbative expression leads to consistent estimates of the magnetic coupling. It has been suggested recently that the reduction of the magnetic coupling parameter to its kinetic exchange part only (the second term in Eq. 3) leads to poor estimates of J when the t parameter is extracted from the doped cluster [91].

However, Table 7 shows that the complete equation gives excellent result when the hopping parameter from the undoped clusters is used. In all cases the IDDCI magnetic coupling (J_{var}) is reproduced within a few milli-electron volts with the perturbative expression. For the linear Cu–O–Cu magnetic interactions paths, the kinetic exchange is the leading term and only a small (but not completely negligible) contribution is observed of the direct exchange. For the interladder interactions, the magnetic coupling is dominated by the direct exchange, the kinetic exchange is almost reduced to zero. On the other hand, the rung interaction in $CaCu_2O_3$ is a balance between two comparable contributions. The kinetic exchange is not as dominant as in the rung and leg interactions in the other ladder compounds because of the large deviation from linearity of the Cu–O–Cu linkage, although this contribution is not as small as in the interladder interaction since the angle is still far away from 90°.

Table 6 IDDCI estimates of the direct exchange K (in meV), neutral-ionic hopping parameter t_0 (in meV) and on-site repulsion U (in eV) for $SrCu_2O_3$, $CaCu_2O_3$ and $Sr_2Cu_3O_5$

		$SrCu_2O_3$		$CaCu_2O_3$	$Sr_2Cu_3O_5$
		Idealized	Refined		
K	Leg	2.9	3.6	4.6	4.8/6.4
	Rung	5.4	3.9	8.8	16.5
	Inter	17.4	19.1	14.6	17.3
t_0	Leg	−547	−556	−499	−550/− 545
	Rung	−500	−462	−223	−561/− 530
	Inter	0.7	59.2	36.2	1.8
U	Leg	6.1	6.2	6.5	5.9/5.7
	Rung	6.0	6.3	6.8	5.5/6.2
	Inter	5.2	5.3	5.4	5.2

The two values for $Sr_2Cu_3O_5$ correspond to the inner and outer leg, respectively.

Table 7 Estimates of the magnetic coupling parameter with the perturbative superexchange relation

		J_F	J_{AF}	J_{pert}	J_{var}
$SrCu_2O_3$	Leg	5.88	−197	−191	−186
(idealized)	Rung	10.7	−164	−154	−150
	Inter	34.9	−0.0	34.9	34.9
$SrCu_2O_3$	Leg	7.16	−199	−192	−186
(refined)	Rung	7.86	−135	−127	−125
	Inter	38.2	−2.7	35.5	35.5
$CaCu_2O_3$	Leg	9.2	−152	−143	−139
	Rung	17.5	−29.0	−11.5	−11.5
	Inter	29.2	−1.0	28.2	28.2
$Sr_2Cu_3O_5$	Leg	9.5	−206	−197	−190
	Leg−2	12.9	−206	−193	−186
	Rung	33.0	−203	−170	−165
	Inter	34.5	−0.0	34.5	34.5

The perturbative estimate J_{pert} is decomposed in its ferromagnetic and antiferromagnetic (J_F and J_{AF}) components. Variational IDDCI estimates are added for comparison. All values in meV

4.4 Four-spin cyclic exchange

Rectangular four-center Cu_4O_{12} clusters have been used to determine the cyclic exchange terms in these systems. For $SrCu_2O_3$, we use the idealized crystal structure. As mentioned above, the evaluation of these effective parameters requires the combination of the energy eigenvalues and the wave functions of the six states implicated, by means of the Effective Hamiltonian Theory. These states arise from the combination of the six $S_z = 0$ determinants resulting from the distribution of four spins on four centers. All the information required can be obtained from truncated CI calculations (extended-CAS + single excitations). Details regarding this strategy can be found in Refs. [58, 59]. Besides the four-body cyclic terms, these calculations supply estimates of the third neighbor interactions J_{diag} (cf. Table 2) and provide us additional information about the dependency of the second neighbor magnetic coupling constants on the cluster size.

Three different four-body terms can be distinguished, as shown in Fig. 8: a circular movement of the four spins in the plaquette (J_{ring1}, upper part of Fig. 8), a simultaneous exchange along the legs (J_{ring2}, middle part of Fig. 8) and a simultaneous exchange across the rungs (J_{ring3}, lower part of Fig. 8). Following perturbation theory based arguments

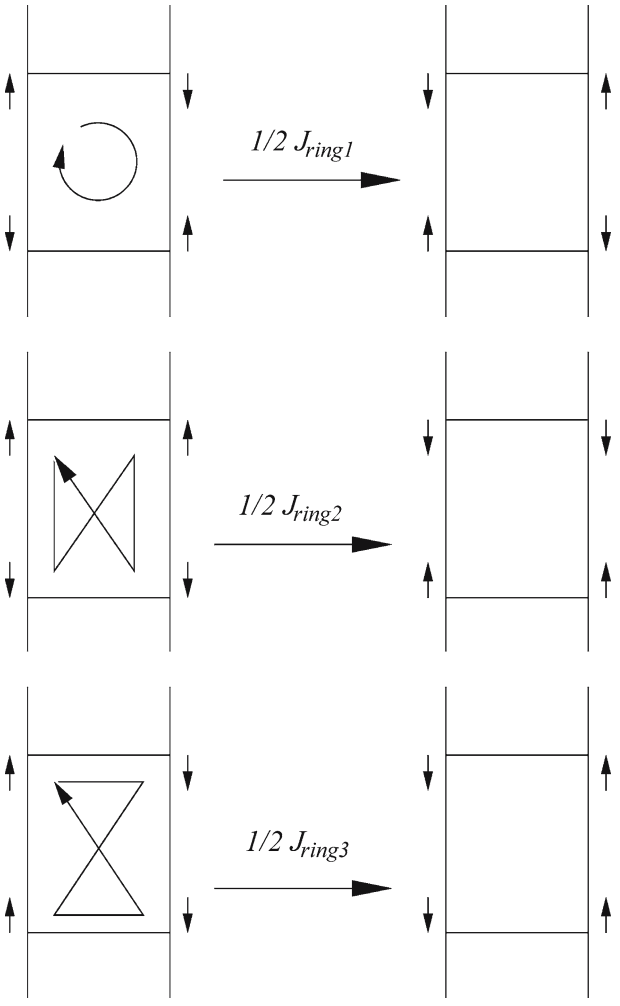

Fig. 8 The three four-body terms: *upper* circular movement of the electrons, J_{ring1}; *middle* simultaneous exchange along the legs, J_{ring2}; and *lower* simultaneous exchange across the rungs, J_{ring3}

it is possible to derive the following relations between the four-spin exchange terms and the two-body interactions (J_{leg}, J_{rung} and J_{diag}) [40,79]:

$$J_{\text{ring1}} = 80\frac{t_{\text{leg}}^2 t_{\text{rung}}^2}{U^3} \simeq \frac{5J_{\text{leg}}J_{\text{rung}}}{U}, \tag{6a}$$

$$J_{\text{ring2}} = 80\frac{t_{\text{leg}}^2 t_{\text{diag}}^2}{U^3} \simeq \frac{5J_{\text{leg}}J_{\text{diag}}}{U}, \tag{6b}$$

$$J_{\text{ring3}} = 80\frac{t_{\text{rung}}^2 t_{\text{diag}}^2}{U^3} \simeq \frac{5J_{\text{rung}}J_{\text{diag}}}{U}, \tag{6c}$$

$$\frac{J_{\text{ring2}}}{J_{\text{ring1}}} = \frac{J_{\text{diag}}}{J_{\text{rung}}}, \tag{7a}$$

$$\frac{J_{\text{ring3}}}{J_{\text{ring1}}} = \frac{J_{\text{diag}}}{J_{\text{leg}}}, \tag{7b}$$

where the direct exchange contributions to the two-body interactions have been neglected.

Table 8 Four-spin cyclic terms (in meV) for $SrCu_2O_3$, $CaCu_2O_3$ and $Sr_2Cu_3O_5$

	$SrCu_2O_3$	$CaCu_2O_3$	$Sr_2Cu_3O_5$
J_{ring1}	34	4	39
J_{ring2}	4.1	1.3	4.1
J_{ring3}	2.7	$\sim 10^{-2}$	3.3
$J_{\text{ring1}}/J_{\text{rung}}$	0.23	0.35	0.22
$5\frac{J_{\text{leg}}J_{\text{rung}}}{U}$	23.0	1.2	28.2
$5\frac{J_{\text{leg}}^{\text{AF}}J_{\text{rung}}^{\text{AF}}}{U}$	26.7	3.3	35.9
$J_{\text{ring2}}/J_{\text{ring1}}$	0.120	0.325	0.105
$J_{\text{diag}}/J_{\text{rung}}$	0.087	0.035	0.080
$J_{\text{ring3}}/J_{\text{ring1}}$	0.079	0.002	0.085
$J_{\text{diag}}/J_{\text{leg}}$	0.070	0.003	0.074

Table 8 reports the variationally determined J_{ring} values as well as the perturbative estimates, i.e. the outcomes of Eq. 6 using the IDDCI values listed in Table 6 and 7. In $SrCu_2O_3$ and $Sr_2Cu_3O_5$, the J_{ring1} term is around 35 meV, larger than for the two-dimensional (2D) La_2CuO_4 cuprate (14 meV). [59,58] The folding of the Cu–O–Cu rung angle in

$CaCu_2O_3$ system affects the four-spin cyclic term, which adopts here a value of only 4 meV, significantly smaller than in the rest of the systems considered here. The parameters J_{ring2} and J_{ring3} are small in all cases, especially for $CaCu_2O_3$ due to the distortion introduced by the buckling of the lattice. The J_{ring1}/J_{rung} ratio is around 0.3, in rather good agreement with the value suggested by Brehmer et al. [7] from their perturbative analysis and the value proposed by Matsuda et al. [8] (Due to the different definition of the four-spin cyclic exchange used by Matsuda and co-workers, the value of J_{ring} should be multiplied by 2 to compare with the present results) for the two-legged ladder $La_6Ca_8Cu_{24}O_{41}$. The latter copper oxide compound has a layered structure in which Cu_2O_3 ladder planes similar to those in $SrCu_2O_3$ are alternated with CuO_2 spin chain layers [80].

Table 8 shows that the ratios J_{ring2}/J_{ring1} and J_{ring3}/J_{ring1} compare rather well with the ratios J_{diag}/J_{rung} and J_{diag}/J_{leg} for Sr ladders, as predicted by Eq. 7. This indicates that Eqs. 6 and 7 are useful expressions to analyze the enhancement of the four-body terms in the strontium spin ladders with respect to two-dimensional cuprates. The increase of J_{ring1} coincides with an increase of the second neighbor coupling constants (J_{rung} and J_{leg} in Table 7 to be compared with $J = -130$ meV in La_2CuO_4[23–27]) and a decrease of the on-site Coulomb repulsion U (values in Table 6 with respect to $U = 7.4$ eV in La_2CuO_4[54]).

The decrease of the on-site Coulomb repulsion U by approximately 1 eV contradicts the usual assumption that this parameter is material independent (see for instance, Ref. [81]). The smaller U in the spin ladders is probably due to the polarization effects in the solid, which will be different depending on the specific structure of the system.

The increase of J should be interpreted as a subtle interplay between changes in U, the hopping integral t_{pd} and the charge transfer energy Δ as shown by the fourth-order perturbation theory expression of the AF contribution to J (cf. Fig. 4):

$$J_{AF} \propto -\frac{t_{pd}^4}{\Delta^2 U}. \tag{8}$$

t_{pd} corresponds to the hopping between the bridging O-2p and the Cu-3d orbitals, and Δ is the energy associated to the transfer of an electron from the ligand to a Cu-3d orbital. The ferromagnetic contribution to J can be assumed to be almost constant in the ladders and the 2D cuprates given that the variation in the Cu–Cu distance, the determining factor in the size of the direct exchange, is not large enough to cause significant changes in this parameter.

The hopping integral t_{pd} decreases exponentially with the Cu–O distance [82–84]. Since mean Cu–O distances are slightly larger in ladder than in 2D cuprates, it can be expected that $t_{pd}^{ladder} \leq t_{pd}^{2D}$. There is, however, an additional factor controlling the hopping integral, namely the difference in Madelung potential at Cu and O sites Δ_{Mad}. When this difference increases, the energy difference between the O-2p and Cu-3d orbitals is also enhanced. This produces a less efficient 2p-3d overlap and, consequently, a reduction of the t value [85].

Table 9 Madelung potential (in eV) at atomic sites for the 2D AFM La_2CuO_4; the spin ladders $SrCu_2O_3$, $CaCu_2O_3$, and $Sr_2Cu_3O_5$; and the 1D spin chain Sr_2CuO_3

Atom	La_2CuO_4	$SrCu_2O_3$	$CaCu_2O_3$	$Sr_2Cu_3O_5$	Sr_2CuO_3
Cu	−28.62	−24.38	−24.18	−24.73[a], −24.27[b]	−24.17
O_r	20.98	21.35	23.22	21.32	–
O_l	20.98	22.45	22.82	21.18[a], 22.45[b]	20.08
Cation	−27.95	−19.67	−21.44	−19.71	19.74
$\Delta_{Mad}(O_r\text{-Cu})$	49.6	45.73	47.40	46.05[a], 45.59[b]	–
$\Delta_{Mad}(O_l\text{-Cu})$	49.6	46.82	47.00	45.91[a], 46.72[b]	44.25

O_r and O_l refer to the oxygens located on the rung and leg, respectively. Δ_{Mad} corresponds to the difference in Madelung potential at O and Cu sites

[a] Inner leg

[b] Outer leg.

Table 9 shows that Δ_{Mad} is larger for La_2CuO_4 than for the rest of systems. As a result of these two opposite effects, t values are only slightly affected by the material as shown in Table 6.

The charge transfer energy Δ is also strongly affected by the difference in Madelung potential at Cu and O sites:

$$\Delta = \Delta_{Mad} - E_I(Cu) - E_A(O) - E_{pol}, \tag{9}$$

where $E_I(Cu)$ represents the atomic ionization energy of the Cu atom, $E_A(O)$ the second electron affinity of oxygen and E_{pol} the screening energy due to the polarizability of the oxygen anions [86]. Neglecting the differences in the oxygen polarizability in the different environments, it is possible to correlate directly the charge transfer energy with the difference in Madelung potential; a large Δ_{Mad} gives a large Δ, which in turn leads to smaller J_{AF}. La_2CuO_4 presents the largest difference in the Madelung potential at Cu and O sites and indeed the smallest J value. In summary, the increase of U and Δ_{Mad} and the stable value of t_{pd} are in agreement with the larger two-body interactions and the four-body terms in the strontium ladders with respect to the 2D cuprates.

In line with this rather simple analysis of the increase of J in the spin ladders with respect to the 2D cuprates, we can also explain why this parameter is still larger in the 1D spin chain compound Sr_2CuO_3, $J \sim -245$ meV [41,87,88]. For this compound, Δ_{Mad} is still smaller than in the ladder cuprates (see last column of Table 9) and U is also slightly smaller (5.8 eV). This results in a smaller denominator in Eq. 8, and hence a larger J can be expected.

5 Summary and concluding remarks

The particular crystal structure of the spin ladder compounds gives rise to a large number of different interactions between the Cu^{2+} centers in the lattice. Ab initio calculations by means of the IDDCI scheme on properly embedded cluster models are applied to extract information about these interactions. For the magnetic coupling, the second-neighbor interactions are dominant, but first-neighbor and third-neighbor

interactions are non-negligible. The interactions along linear Cu–O–Cu paths are slightly larger than in the 2D cuprate La_2CuO_4 whereas the buckling of the ladder planes in the calcium ladder strongly reduces the interaction along the rungs. Hence, this compound is better understood as a quasi-1D spin chain, although the interchain interactions (J_{rung} and J_{inter}) are not so small as in Sr_2CuO_3 or Li_2CuO_2, two compounds with significantly lower Néel temperature (5.4 and 9.4 K) [89,90] than the ~ 25 K for $CaCu_2O_3$ [49]. The same conclusions hold for relative sizes of the hopping parameters calculated from the doped clusters.

The effective parameters that define the valence Hamiltonian for magnetic coupling (U, t_0 and K) are extracted from the IDDCI calculations using the effective Hamiltonian theory. Especially interesting is the observation that the ts derived from the undoped clusters deviate substantially for the corresponding parameters obtained from the doped clusters. Furthermore, we observe that the direct exchange, although small, is not negligible. This has important consequences on the applicability of the superexchange relation $J = 2K - 4t^2/U$. Often, the direct exchange is not considered and t is taken as the parameter that measures the mobility of the holes, i.e., the value of the doped clusters. This simplification leads to unreliable estimates of J, whereas the correct usage of the formula gives perturbative estimates in perfect agreement with the IDDCI J values.

The four-body interactions in the strontium ladders is found to be larger than the ones in the copper oxide planes in La_2CuO_4. An analysis based on the perturbation theory arguments shows that this is inherent to the more antiferromagnetic interactions along the leg and rung in the spin ladders. This increase of the magnetic coupling is related to the differences in the Madelung potential between the 2D cuprates and the spin ladders. The increase of the Madelung potential (i.e., less negative value) on the copper sites explains the smaller U in the spin ladders, and the decrease in the difference between the Madelung potential on copper and oxygen sites lowers the ligand to metal charge transfer energy. Both effects are in line with a more antiferromagnetic interaction.

Acknowledgements The authors have had the privilege to collaborate with Jean-Paul Malrieu in various occasions and to share his inexhaustible enthusiasm, creativity and perception of science, always oriented towards the understanding of physics. We want to express our profound gratitude for this. Financial support has been provided by the Spanish Ministry of Science and Technology under Project No. BQU2002-04029-C02-02 and the DURSI of the Generalitat de Catalunya (grant SGR01-00315).

References

1. Zhang FC, Rice TM (1988) Phys Rev B 37:3759
2. Hybertsen MS, Stechel EB, Schluter M, Jennison DR (1990) Phys Rev B 41:11068
3. Jefferson JH, Eskes H, Feiner LF (1992) Phys Rev B 45:7959
4. Nazarenko A, Vos KJE, Haas S, Dagotto E, Gooding RJ (1995) Phys Rev B 51:8676
5. Eroles J, Batista CD, Bacci SB, Gagliano ER (1999) Phys Rev B 59:1468
6. Lorenzana J, Eroles J, Sorella S (1999) Phys Rev Lett 83:5122
7. Brehmer S, Mikeska H-J, Müller M, Nagaosa N, Uchida S (1999) Phys Rev B 60:329
8. Matsuda M, Katsumata K, Eccleston RS, Brehmer S, Mikeska H-J (2000) Phys Rev B 62:8903
9. Gößling A, Kuhlmann U, Thomsen C, Löffert A, Gross C, Assmus W (2003) Phys Rev B 67:052403
10. Johnston DC (1996) Phys Rev B 54:13009
11. Eccleston RS, Uehara M, Akimitsu J, Eisaki H, Motoyama N, Uchida S (1998) Phys Rev Lett 81:1702
12. Sakai T (2001) Phys Rev B 63:140509
13. Himeda Y, Kato T, Ogata M (2002) Phys Rev Lett 88:117001
14. Anisimov VI, Korotin MA, Nekrasov IA, Pchelkina ZV (2002) Phys Rev B 66:100502
15. Tipper JM, Vos KJE (2003) Phys Rev B 67:144511
16. Guo GY, Temmermann WM (1998) J Phys C 21:L803
17. Pickett WE (1989) Rev Mod Phys 61:433
18. Matheiss LF (1994) Phys Rev B 49:14050
19. Rosner H, Eschrig H, Hayn R, Drechsler S-L, Málek J (1997) Phys Rev B 56:3402
20. Martin RL, Illas F (1997) Phys Rev Lett 79:1539
21. Illas F, Martin RL (1998) J Phys Chem 108:2519
22. van Oosten AB, Broer R, Nieuwpoort WC (1996) Chem Phys Lett 257:207
23. Calzado CJ, Sanz JF, Malrieu J-P, Illas F (1999) Chem Phys Lett 307:102
24. Moreira IdePR, Illas F, Calzado CJ, Sanz JF, Malrieu J-P, Ben Amor N, Maynau D (1999) Phys Rev B 59:6593
25. Calzado CJ, Sanz JF, Malrieu J-P (2000) J Chem Phys 112:5158
26. Aeppli G, Hayden SM, Mook HA, Fisk Z, Cheong S-W, Rytz D, Remeika JP, Espinosa GP, Cooper AS (1989) Phys Rev Lett 62:2052
27. Sulewski PE, Fleury PA, Lyons KB, Cheong C-W, Fisk Z (1990) Phys Rev B 41:225
28. Anisimov VI, Zaanen J, Anderson OK (1991) Phys Rev B 44:943
29. Czyzyk MT, Sawatzky GA (1994) Phys Rev B 49:14211
30. Moreira IdePR, Illas F, Martin RL (2002) Phys Rev B 65:155102
31. Cabrero J, Calzado CJ, Maynau D, Caballol R, Malrieu J-P (2002) J Phys Chem A 106:8146
32. Yang Z, Huang Z, Ye L, Xie X (1999) Phys Rev B 60:15674
33. Dagotto E, Rice TM (1996) Science 271:618
34. Rice TM (1997) Z Phys B 103:165
35. Maekawa S (1996) Science 273:1515
36. Dagotto E, Riera J, Scalapino DJ (1992) Phys Rev B 45:5744
37. White SR, Noack RM, Scalapino DJ (1994) Phys Rev Lett 73:886
38. Azuma M, Hiroi Z, Takano M, Ishida K, Kitaoka Y (1994) Phys Rev Lett 73:3463
39. de Graaf C, Moreira IdePR, Illas F, Martin RL (1999) Phys Rev B 60:3457
40. Calzado CJ, de Graaf C, Bordas E, Caballol R, Malrieu J-P (2003) Phys Rev B 67:132409
41. de Graaf C, Illas F (2001) Phys Rev B 63:014404
42. Kim TK, Rosner H, Drechsler S-L, Hu Z, Sekar C, Krabbes G, Málek J, Knupfer M, Fink J, Eschrig H (2003) Phys Rev B 67:024516
43. Ricart JM, Dovesi R, Roetti C, Saunders VR (1995) Phys Rev B 52:2381
44. Moreira IdePR, Illas F (1997) Phys Rev B 55:4129
45. Su Y-S, Kaplan TA, Mahanti SD, Harrison JF (1999) Phys Rev B 59:10521
46. Muñoz D, Moreira IdePR, Illas F (2002) Phys Rev B 65:224521
47. Winter NW, Pitzer RM, Temple DK (1987) J Chem Phys 86:3549
48. Hiroi Z, Azuma M, Takano M, Bando Y (1991) J Solid State Chem 95:230
49. Kiryukhin V, Kim YJ, Thomas KJ, Chou FC, Erwin RW, Huang Q, Kastner MA, Birgeneau RJ (2001) Phys Rev B 63:5122
50. Miralles J, Daudey JP, Caballol R (1992) Chem Phys Lett 198:555
51. Miralles J, Castell O, Caballol R, Malrieu J-P (1993) Chem Phys 172:33
52. de Graaf C, Sousa C, Moreira IdePR, Illas F (2001) J Phys Chem A 105:11371

53. Cabrero J, de Graaf C, Bordas E, Caballol R, Malrieu, J-P (2003) Chem Eur J 9:2307
54. Calzado CJ, Cabrero J, Malrieu J-P, Caballol R (2002) J Chem Phys 116:3985
55. Guihery N, Malrieu JP (2003) J Chem Phys 119:8956
56. de Graaf C, Hozoi L, Broer R (2004) J Chem Phys 120:961
57. García VM, Castell O, Caballol R, Malrieu J-P (1995) Chem Phys Lett 238:222
58. Calzado CJ, Malrieu J-P (2001) Eur Phys J B 21:375
59. Calzado CJ, Malrieu J-P (2001) Phys Rev B 63:214520
60. Gellé A, Munzarová ML, Lepetit MB, Illas F (2003) Phys Rev B 68:125103
61. Widmark P-O, Malmqvist P-Å, Roos BO (1990) Theor Chim Acta 77:291
62. Pou-Amérigo R, Merchán M, Nebot-Gil I, Widmark PO, Roos BO (1995) Theor Chim Acta 92:149
63. Andersson K, Barysz M, Bernhardsson A, Blomberg MRA, Cooper DL, Fleig T, Fülscher MP, de Graaf C, Hess BA, Karlström G, et al (2002) MOLCAS version 5.4. Department of Theoretical Chemistry, University of Lund
64. Maynau D, Ben Amor N (1997) CASDI suite of programs. Department of Quantum Physics, University Paul Sabatier, Toulouse
65. de Graaf C, Moreira IdePR, Illas F, Iglesias O, Labarta A (2002) Phys Rev B 66:014448
66. Illas F, Moreira IdePR, de Graaf C, Castell O, Casanovas J (1997) Phys Rev B 56:5069
67. Calzado CJ, Cabrero J, Malrieu J-P, Caballol R (2002) J Chem Phys 116:2728
68. Azaria P, Lecheminant P, Nersesyan AA (1998) Phys Rev B 58:8881
69. Weihong Z, Kotov V, Oitmaa J (1998) Phys Rev B 57:11439
70. Zhu N, Wang X, Chen C (2001) Phys Rev B 63:012401
71. Hayden SM, Aeppli G, Osborn R, Taylor AD, Perring TG, Cheong S-W, Fisk Z (1991) Phys Rev Lett 67:3622
72. Uehara M, Nagata T, Akimitsu J, Takahashi H, Mori N, Kinoshita K (1996) J Phys Soc Jpn 65:2764
73. Calzado CJ, Malrieu J-P (2000) Chem Phys Lett 317:404
74. Anderson PW (1959) Phys Rev 115:2
75. Hay PJ, Thibeault JC, Hoffmann RJ (1975) J Am Chem Soc 97:4884
76. Kahn O, Briat BJ (1976) J Chem Soc Faraday Trans 72:268
77. Bloch C (1958) Nucl Phys 6:329
78. Malrieu J-P, Durand P, Daudey J-P (1985) J Phys A 18:809
79. Calzado CJ, Malrieu J-P (2004) Phys Rev B 69:094435
80. Siegriest T, Schneemeyer LF, Sunshine SA, Waszczak, JV (1988) Mat Res Bull 23:1429
81. Mizuno Y, Tohyama T, Maekawa S (1998) Phys Rev B 58:14713
82. Closs GL, Miller JR (1988) Science 240:440
83. Newton MD (1991) Chem Rev 91:767
84. Jordan KD, Paddon-Row MN (1992) Chem Rev 92:395
85. Wolfsberg M, Helmholz L (1952) J Chem Phys 20:395
86. Zaanen J, Sawatzky GA (1990) J Solid State Chem 88:8
87. Takigawa M, Motoyama N, Eisaki H, Uchida S (1996) Phys Rev Lett 76:4612
88. Lorenzana J, Eder R (1997) Phys Rev B 55:3358
89. Sapiña F, Rodríguez-Carvajal J, Sanchis MJ, Ibáñez R, Beltrán A, Beltrán D (1990) Solid State Commun 74:779
90. Ami T, Crawford MK, Harlow RL, Wang ZR, Johnston DC, Huang Q, Erwin RW (1995) Phys Rev B 51:5994
91. Bordas E, de Graaf C, Caballol R, Calzado CJ (2005) Phys Rev B 71:045108